

## Numerical study of effect of hydrogen content on the structure of syngas diffusion flame

Priyanka Swarnkar\*, Akhilesh Kumar Sahu and T. Sundararajan

Department of Mechanical Engineering, Indian Institute of Technology Madras, Chennai, 600036, India

\*Corresponding author: [priyankaswarnkar.swarnkar@gmail.com](mailto:priyankaswarnkar.swarnkar@gmail.com)

### ABSTRACT

Syngas, produced during gasification reactions, primarily is composed of carbon-monoxide (CO) and hydrogen (H<sub>2</sub>), along with other gases like carbon-dioxide (CO<sub>2</sub>), nitrogen (N<sub>2</sub>) and methane (CH<sub>4</sub>). The composition of these gases produced during gasification varies with the type of fuel, oxidizer concentration, operational pressure and temperature. For instance, the amount of CO produced during the endothermic reactions depends strongly on the temperature. The flame structure for different syngas compositions would be an important input for designing a good syngas burner. This paper is an attempt to numerically study the effect of varying the hydrogen concentration in syngas, on the resulting flame structure. A straight cylindrical tube of 4 mm diameter has been considered as the burner tube. Length has been chosen such that flow completely develops within the tube. The jet emerging at the exit of the tube entrains air naturally and the flow is laminar. An axi-symmetric model with simplified Davis mechanism (detailed chemistry mechanism consisting of fourteen species) has been used. A detailed examination of the reaction zone indicates that along the radial direction, CO oxidation occurs followed by the formation of water vapor. The higher species diffusivity and kinetic rate coefficient values for the hydrogen- oxygen reaction over those of CO play a crucial role in determining the overall syngas flame characteristics.

### KEYWORDS

Syngas; flame structure; non-premixed flame; numerical simulation; detailed chemical kinetics

### INTRODUCTION

Due to the increased demand and depletion of fossil fuels, there is a need for alternative fuels. Various researchers have focused their attention towards solid fuels such as coal and biomass, which are abundantly available worldwide. In order to provide a clean energy source and to reduce carbon foot print,

Integrated Gasification Combined Cycle (IGCC) technology has been introduced to achieve higher efficiency and lower emissions. The IGCC power plants allow the gasification of wide range of liquid and solid fuels and even waste-derived materials to convert into fuel gas mixtures that can be used in the gas turbine to generate electricity [1]. In an IGCC power plant, the solid and liquid fuels are gasified and the evolved gas is called syngas. The syngas is composed of many gaseous constituents, chief ones being CO and H<sub>2</sub>, along with other gases like H<sub>2</sub>O, CO<sub>2</sub>, N<sub>2</sub> and CH<sub>4</sub> [2]. The composition of syngas varies largely, depending on the fuel resource (biomass and different types of coal), type of gasification and processing conditions. Hydrogen mole fraction in syngas varies from 9% to 40% in a typical IGCC plant fueled by coal, biomass or solid waste [3]. Also the mole fraction of hydrogen in a coal-based IGCC power plant for typical processing conditions was reported to vary from 25% to 70% [4]. The variation of syngas composition has great influence on the combustion process, and hence is a challenge for combustor design. Several research works have been reported on the fundamental combustion characteristics of syngas ignition delay [7, 8] and flame speed [9, 10], and also on the development of detailed chemical reaction mechanisms [11, 12]. Various studies on the combustion properties such as adiabatic flame temperature and flammability limits have also been carried out. Measurement of laminar burning velocity which is an important characteristic of the fuel mixture and which governs the structure and stability of premixed flames, has also been reported [2, 5, 6]. The presence of Hydrogen in the fuel mixture affects the flame speed and structure, because of its high laminar burning velocity as compared to the other gaseous fuels [13, 14, and 15]. Considerable amount of data is available in literature on the effects of fuel properties on flame speed. However, the research work available is limited with respect to the flame structure of low calorific value multi-component fuels. Particularly, the effects of diluents such as CO<sub>2</sub> and N<sub>2</sub> on the combustion process of low calorific

value syngas are not addressed. Therefore, in this paper, numerical study of the behavior of diffusion flame over a wide range of  $H_2/CO$  ratios is presented. The changes in flame structure due to variations in the  $H_2$  concentration are investigated, to be of use in the design of syngas burners.

## NOMENCLATURE

- $D$  Binary mass diffusion coefficient  
 $\vec{g}$  Gravitational acceleration vector ( $m/s^2$ )  
 $\Delta h_f$  Enthalpy of formation ( $J/kg$ )  
 $I$  Unit tensor  
 $\vec{j}$  Diffusive mass flux of species ( $kg/ms^2$ )  
 $M_w$  Molecular weight of mixture ( $kg/mol$ )  
 $N$  Total number of species  
 $p$  Static pressure ( $N/m^2$ )  
 $q_R''$  Radiation heat flux  $w/m^3$   
 $R_i$  Net mass rate of production of species ( $kg/m^3s$ )  
 $r^*$  Dimensionless radial distance scaled by internal radius of the burner  
 $X$  Mole fraction  
 $Y$  Mass fraction  
 $z^*$  Dimensionless axial distance scaled by internal radius of the burner  
 $\mu$  Molecular viscosity  
 $\rho$  Density ( $kg/m^3$ )  
 $\vec{\tau}$  Stress tensor ( $N/m^2$ )

## Subscript

i Species

## COMPUTATIONAL DOMAIN

An axi-symmetric, unsteady, pressure based solver has been used to simulate laminar diffusion flames of syngas. Commercial CFD software FLUENT 13 has been used for this purpose. The detailed and optimized chemical mechanism of Davis et al. [13] having 14 species and 38 reaction steps has been used as the chemistry sub-model. The convergence criterion is set as  $10^{-3}$  to  $10^{-6}$  for non-dimensional residues, and overall mass balance has been maintained to less than 1% of the fuel flow rate. The computational domain along with the boundary conditions is shown in Fig. 1. A computational domain extending to 60 diameters (240 mm) in the axial direction and 10 diameters (40 mm) in the radial direction has been considered, for a burner of 4 mm outer diameter. Proper domain independence study has been carried out initially to fix the domain extent.

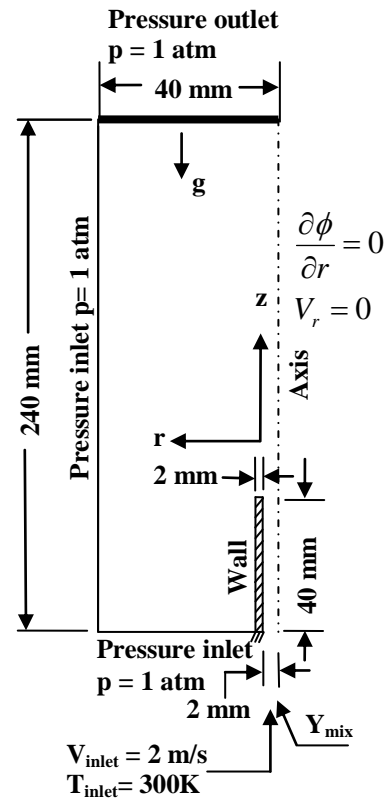


Figure 1: Computational domain and boundary conditions

## GRIDS USED NEAR BURNER

The grid has been created using the commercial software of GAMBIT 2.4.6. A non-uniform rectangular mesh with more than 100,000 cells has been generated and the fine grid region near the burner exit is shown in Fig. 2.

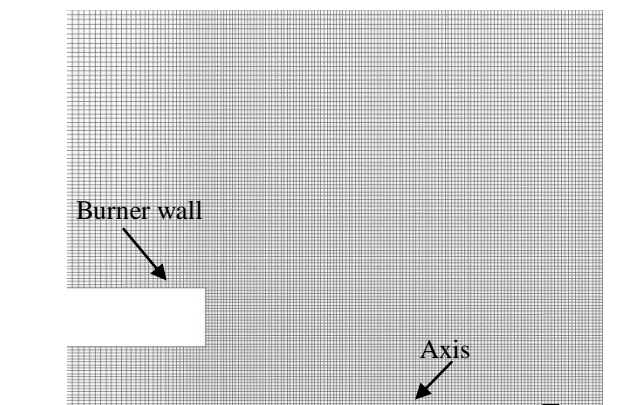


Figure 2: Typical non-uniform grid used near burner exit

The grid size near the exit of the burner is kept as  $2 \cdot 10^{-4}$  m to accurately represent the high gradient regions in the diffusion flame.

### MODEL PARAMETERS

A stainless steel tube burner of 4 mm internal diameter and 8 mm external diameter having a length of 40 mm has been considered. The basic syngas composition employed in this study has been taken from the work of Iyengar and Haque [16], who have investigated the gasification of Indian coals. In order to study the effect of increasing  $H_2$  concentration on the flame structure of syngas, volume percentage of  $H_2$  has been varied from approximately 16% to 26%, keeping the percentages of CO and  $CO_2$  in the syngas constant. With increase in  $H_2$  fraction, the nitrogen content in the fuel mixture is correspondingly reduced. Volumetric composition of the fuel mixture for the three cases considered in this study is reported in Table 1.

Initially the cold flow has been solved and after its convergence, a high temperature zone is patched in a small region near the burner exit to initiate combustion. After obtaining convergence with this, radiation model is turned on using a User Defined Function (UDF) written in C language. Second order discretization methods have been employed to obtain either a converged solutions.

**Table 1:** Syngas composition used in the study

Cases	Syngas composition % by volume and mass fraction is given in brackets			
	$H_2$	CO	$CO_2$	$N_2$
Case 1	16 (0.0123)	15.3 (0.168)	10.7 (0.184)	58 (0.628)
Case 2	21 (0.0173)	15.3 (0.177)	10.7 (0.193)	53 (0.609)
Case 3	26 (0.023)	15.3 (0.187)	10.7 (0.204)	48 (0.584)

### GOVERNING EQUATIONS

The governing equations for the problem are the conservation of mass, momentum, species and energy as given below.

*Continuity equation*

$$\frac{\partial \rho}{\partial t} + (\rho \vec{V}) = 0$$

*Momentum equation*

$$\frac{\partial(\rho \vec{V})}{\partial t} + \nabla \cdot (\rho \vec{V} \vec{V}) = -\nabla p + \nabla \cdot \vec{\tau} + \rho \vec{g}$$

Where

$$\vec{\tau} = \mu[\nabla \vec{V} + \nabla \vec{V}^T - \frac{2}{3} \nabla \cdot \vec{V} I]$$

*Species conservation equations*

$$\frac{\partial(\rho Y_i)}{\partial t} + \nabla \cdot (\rho \vec{V} Y_i) = -\nabla \cdot \vec{J}_i + R_i + S_i$$

Conservation equations have been solved for N-1 active species. The mass fraction of  $N_2$  which is an inert species, is obtained from the identity  $\sum Y_i = 1$ . Full multi-component diffusion is considered. Species velocity is calculated using the Maxwell–Stefan equation.

$$\vec{J}_i = \sum_{j=1}^{N-1} \rho D_{ij} \nabla Y_j$$

Where

$$D_{ij} = [D] = [A]^{-1} [B]$$

$$A_{ii} = -\left( \frac{X_i}{D_{iN}} \frac{M_w}{M_{w,N}} + \sum_{j=1, j \neq i}^N \frac{X_j}{D_{ij}} \frac{M_w}{M_{w,i}} \right)$$

$$A_{ij} = X_i \left( \frac{1}{D_{ij}} \frac{M_w}{M_{w,j}} - \frac{1}{D_{iN}} \frac{M_w}{M_{w,N}} \right)$$

$$B_{ii} = -\left( X_i \frac{M_w}{M_{w,N}} + (1 - X_i) \right) \frac{M_w}{M_{w,N}}$$

$$B_{ii} = X_i \left( \frac{M_w}{M_{w,j}} - \frac{M_w}{M_{w,N}} \right)$$

Here, [A] and [B] are (N-1)×(N-1) matrices.

*Energy equation*

The energy conservation equation consisting of enthalpy transport by species and radiative heat flux losses, is given by

$$\frac{\partial}{\partial t} (\rho C_p T) + \nabla \cdot (\rho \vec{V} C_p T) = \nabla \cdot (K \nabla T) + \sum_{i=1}^N R_i \Delta h_{f,i} + \sum_{i=1}^N [\nabla \cdot (\rho D_{ij} C_{p,i} T \nabla Y_i)] + q_R''$$

## RESULTS AND DISCUSSION

Figure 3 shows the axial temperature variation for three cases with different hydrogen and nitrogen contents in the syngas.

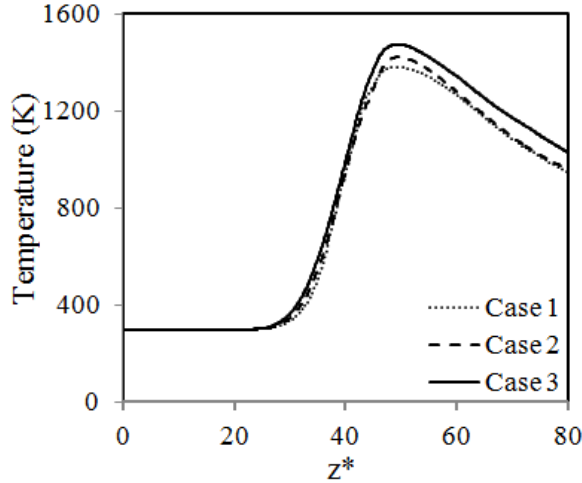


**Figure 3:** Temperature variation along the axis from the burner exit

It is clear from Fig. 3 that the maximum temperature values attained are almost the same for all the three cases. Following literature, the flame height is taken as the axial location at which the maximum temperature is reached. The flame height can be estimated from the high temperature zone seen in the isothermal contour plots (Fig. 4). It is apparent that as the hydrogen content in the fuel is increased from 16% to 21% and then to 26%, the height of the flame increases and flame width also increases radially outwards. This can be attributed to the higher diffusivity and flame speed values for hydrogen.

Radial profiles of the temperature at an axial location of around ( $z^*=15$ ) from the burner exit which is the midplane of the overall flame extent in the axial direction, are shown in Fig. 5. Here also, it is clear that with the increase in hydrogen percentage (from 16%, 21% and 26%) there is a shift in the maximum temperature value from around  $r^*$  value of 1.6 to 1.9. The maximum temperature for case 1 is approximately 200 K less than that for case 3 and the maximum value of case 2 lies in between those of case 2 and case 3.

The radial profiles of mass fractions of hydrogen and oxygen at an axial location of ( $z^*=15$ ) from the burner exit are shown in Fig. 6. It is clear that the hydrogen diffusion zone extends approximately from the  $r^*$  value of 1.4 to 2.2 at that location. Leakage of both fuel and oxygen occur beyond the reaction zone, which is expected in the case of a multi-component

fuel. At higher fraction of hydrogen (case 3), the reaction zone increases in width due to larger leakage of hydrogen.

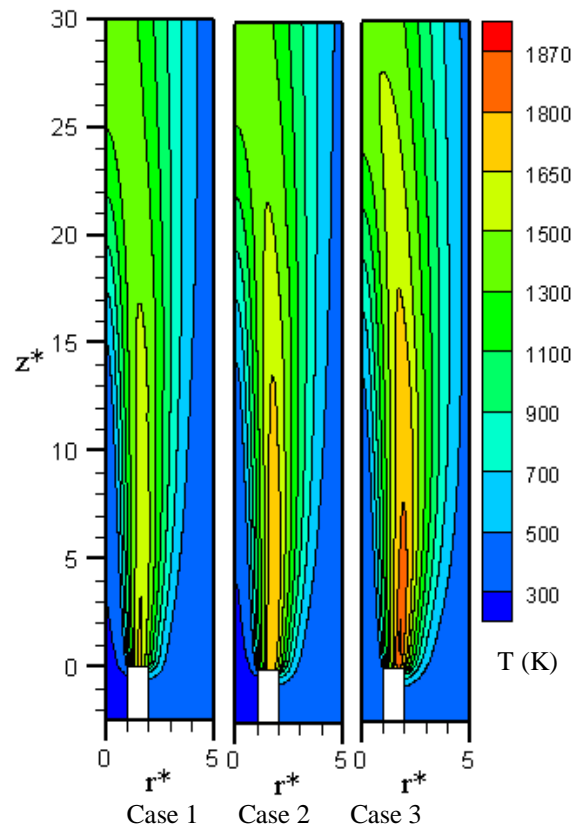


**Figure 4:** Contours of temperature

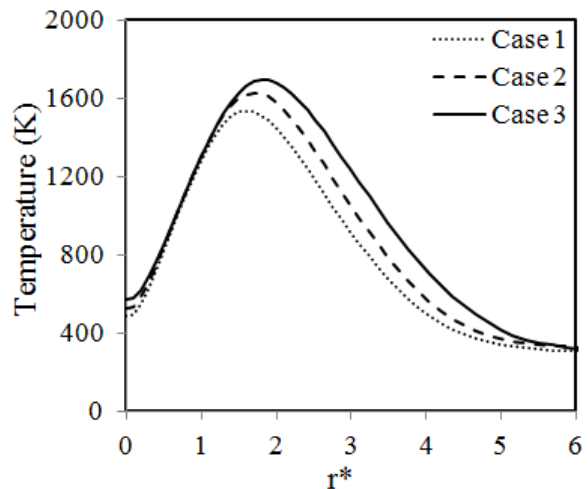


**Figure 5:** Radial temperature profiles at  $z^*=15$

In Figs. 7.a and 7.b, the mass fraction contours and net reaction rate of  $H_2$  are plotted. It is evident that  $H_2$  combustion reactions are completed in an axial distance of about 7-8 diameters from the burner exit.

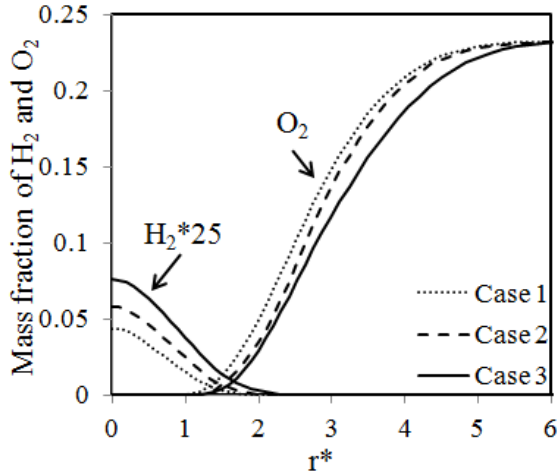


**Figure 6:** Variations of  $H_2$  and  $O_2$  mass fractions along the radial direction at  $z^* = 15$

At a higher hydrogen fraction (case 3), the reaction zone extends to a larger axial extent. From Fig 7.b, it is observed that  $H_2$  gets consumed to form  $H_2O$  and  $OH$  following the reactions  $O + H_2 = H + OH$ ,  $OH + H_2 = H + H_2O$ ,  $H + H + H_2 = H_2 + H_2$  close to the burner tip. Some distance away from the burner exit hydrogen production occurs due to the water gas shift reaction, especially at higher input of  $H_2$  %.

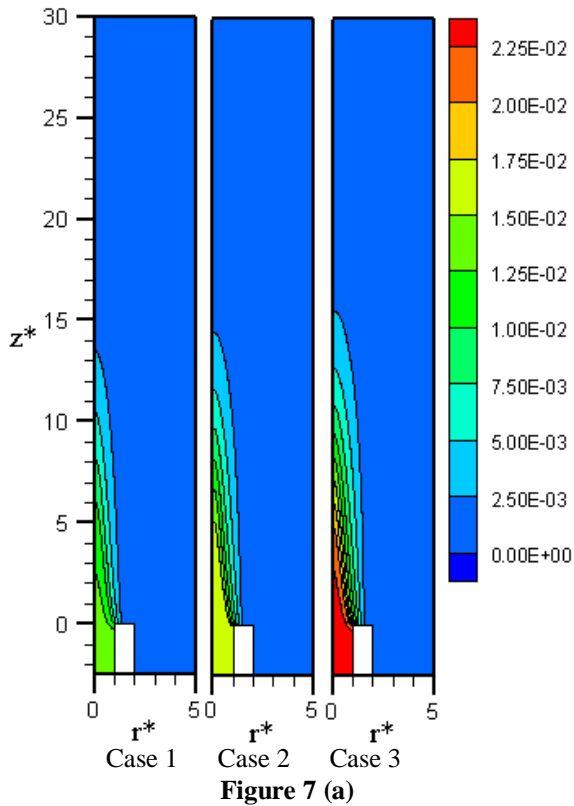


**Figure 7 (a)**

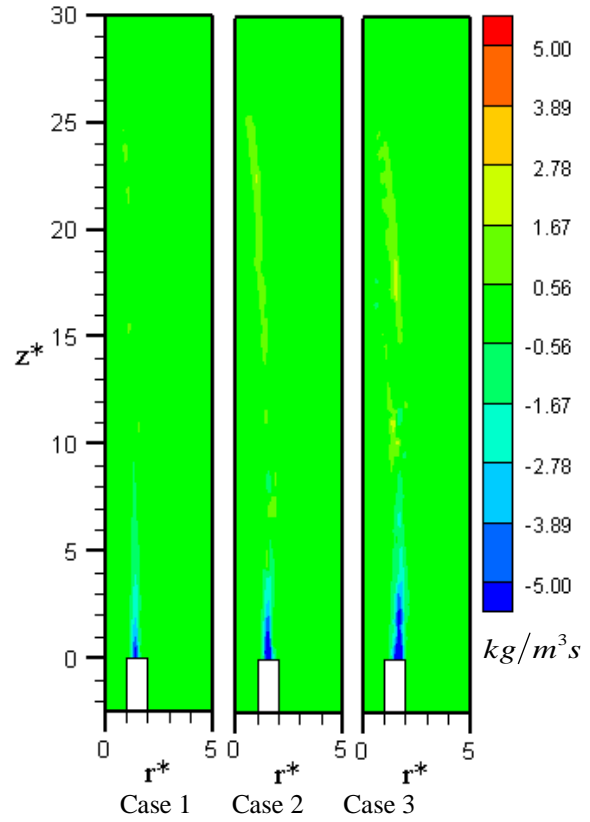


**Figure 7 (b)**

Figure 7: Contours of (a) mass fraction and (b) net reaction rate of  $H_2$

The radial profiles of mass fractions of CO and oxygen at the axial location of  $z^*=15$  from the burner exit are shown in Fig. 8.

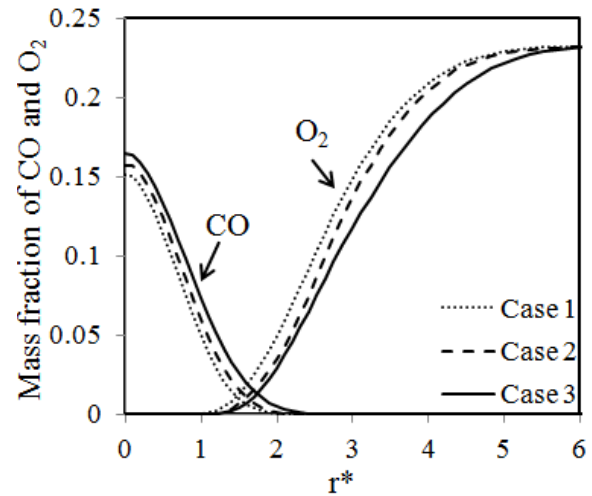


**Figure 8:** Variations of mass fractions of CO and  $O_2$  along the radial direction at  $z^* = 15$

The CO reaction zone is slightly wider than that of H<sub>2</sub> in the radial direction. The CO reaction zone also expands ( $z^* \sim 25$ ) to a larger axial extent than hydrogen (see Fig. 11.a). These can be attributed to the lower flame speed of CO in comparison with hydrogen. If flame speed is less, then a relatively larger flame surface area will be needed, which can be achieved with larger radial and axial extents for the reaction zone.

Radial profiles of CO<sub>2</sub> and H<sub>2</sub>O at the mid-plane of the flame ( $z^*=15$  from the burner exit) are shown in Fig. 9. The maximum value of CO<sub>2</sub> mass fraction occurs closer to the axis at a radial distance of around  $r^*=1.6$ , as a consequence both formation reactions and the presence of CO<sub>2</sub> as a diluent in the fuel mixture. Water vapor is formed slightly away from the axis at around  $r^*=1.95$ . This is due to the higher diffusivity value for hydrogen and also for OH which plays an intermediary role in the formation of H<sub>2</sub>O. The water vapor mass fraction increases with increasing hydrogen content of the fuel; however, the maximum location remains approximately the same.

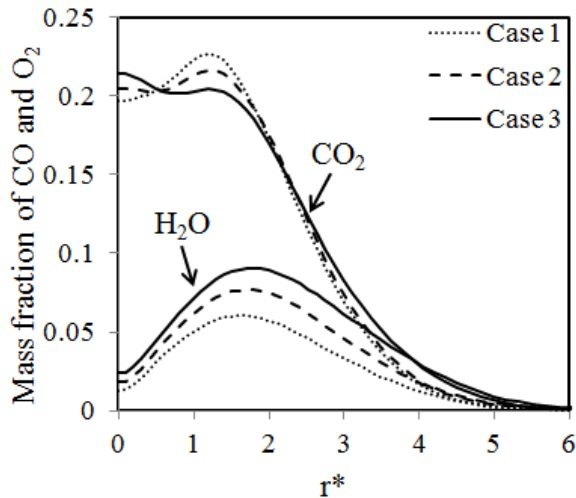


**Figure 9:** Variations of mass fractions of CO<sub>2</sub> and H<sub>2</sub>O along the radial direction at  $z^* = 15$

Figure 10 shows the radial profiles of OH for the three cases at the axial location of  $z^*=15$ . In general, the mass fraction of OH increases with increase in the H<sub>2</sub> fraction of the fuel. The maximum OH location lies in the range  $1.8 < r^* < 2.2$ , closely following the zones of high H<sub>2</sub>O concentration as well as temperature.

In Figs. 11.a and 11.b, the mass fraction contours and the net reaction rates of CO are shown. Although increase in the volume percentage of hydrogen from case 1 to case 3, does not significantly affect the overall features of the CO reaction zone, subtle changes are seen between the three cases. Firstly, at a larger hydrogen volume percentage, the relative

contribution of the CO in terms of its mass fraction increases (Fig. 11.a).

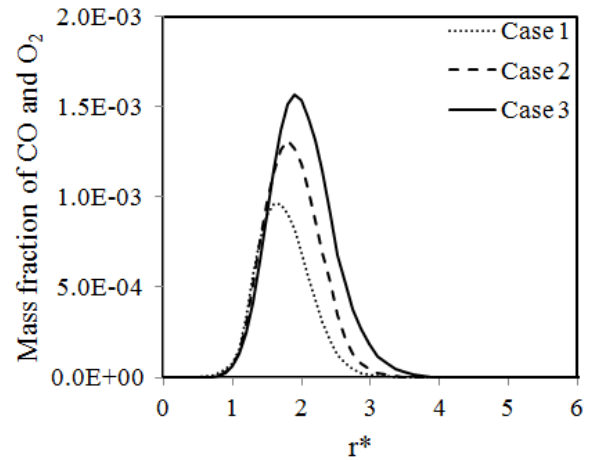


**Figure 10:** Variations of mass fraction of OH along the radial direction at  $z^*=15$

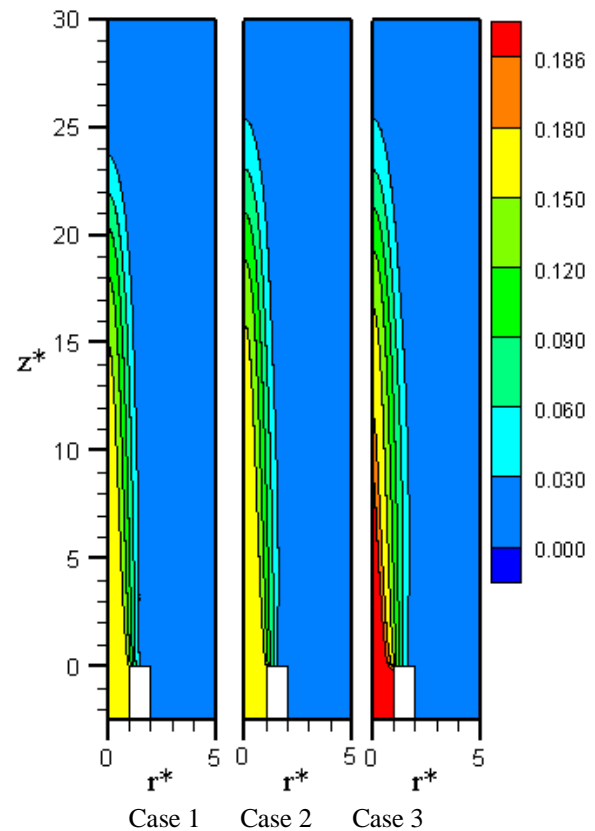


**Figure 11 (a)**

Also, the net reaction rate of CO is mostly negative in magnitude, implying the occurrence of primarily oxidation reactions for CO. However in the high temperature zones, CO production occurs due to CO<sub>2</sub> dissociation (see Fig. 13. b). The consumption of CO (Fig 11.b.) and production of CO<sub>2</sub> (Fig 13.b.) occurs

at the burner rim and gradually moves radially inwards at larger axial distance. This is because of the reactions involved in the system, given as  $\text{CO} + \text{O} + (+\text{M}) = \text{CO}_2 (+\text{M})$ ,  $\text{CO} + \text{O}_2 = \text{CO}_2 + \text{O}$ ,  $\text{CO} + \text{HO}_2 = \text{CO}_2 + \text{OH}$ .

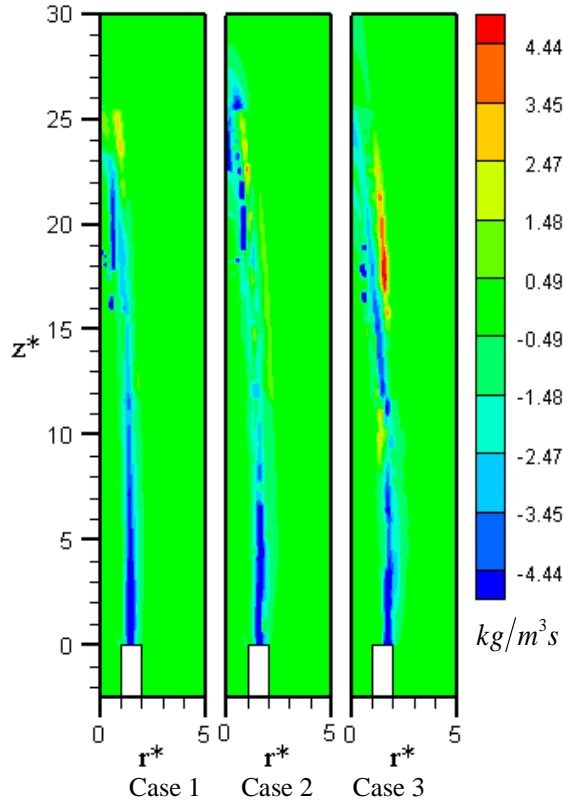


Figure 11 (b)

Figure 11: Contours of (a) mass fraction and (b) net reaction rate of CO

Flame zone expands radially as  $\text{H}_2$  mass fraction in the input mixture is increased. Both the  $\text{O}_2$  mass fraction contours and the net reaction rates of  $\text{O}_2$  shown in Fig. 12.a and 12.b confirm this trend as the percentage of  $\text{H}_2$  changes from 16% to 26%. The reactions  $\text{H} + \text{O}_2 = \text{O} + \text{OH}$  and  $\text{H}_2 + \text{O}_2 = \text{HO}_2 + \text{H}$  cause the consumption of  $\text{O}_2$  to form O, OH,  $\text{HO}_2$ , H. The net reaction rate contours of oxygen (Fig. 12. b) also indicate dissociation reactions to be occurring in the high temperature zones, giving rise to positive  $\text{O}_2$  reaction rates.

In Figs. 13.a and 13.b, the mass fraction contours and net reaction rates of  $\text{CO}_2$  are plotted. The reaction rate contours of  $\text{CO}_2$  closely follow that of CO, indicating that oxidation of CO is the primary route for the formation of  $\text{CO}_2$ . The mass fraction contours of  $\text{CO}_2$  are governed by the amount of  $\text{CO}_2$  present as a diluent in the initial mixture, formation reactions for  $\text{CO}_2$  and the convective and diffusive transport

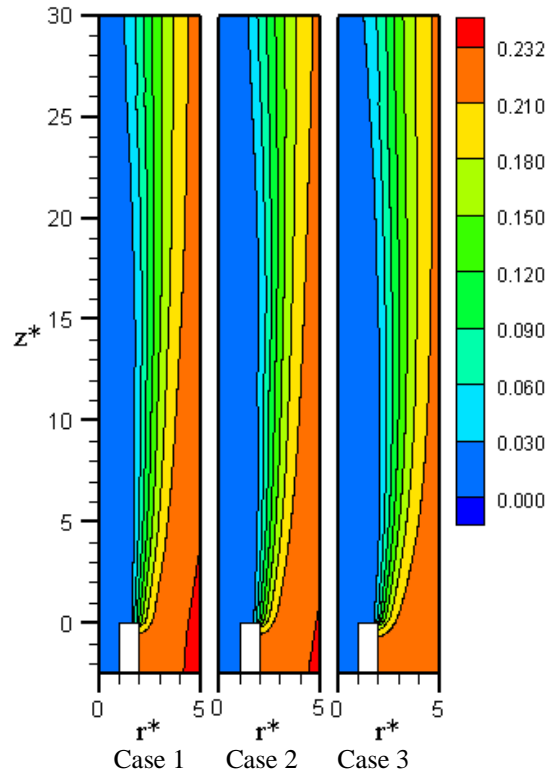


Figure 12 (a)

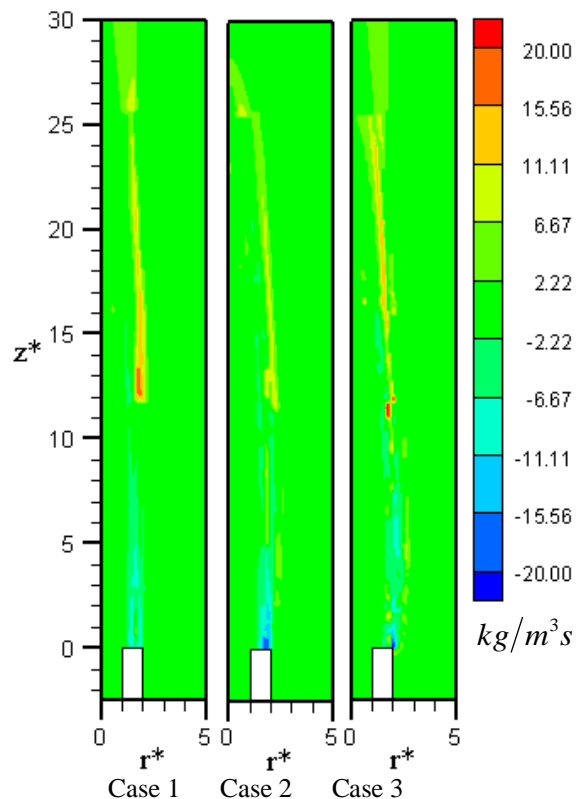
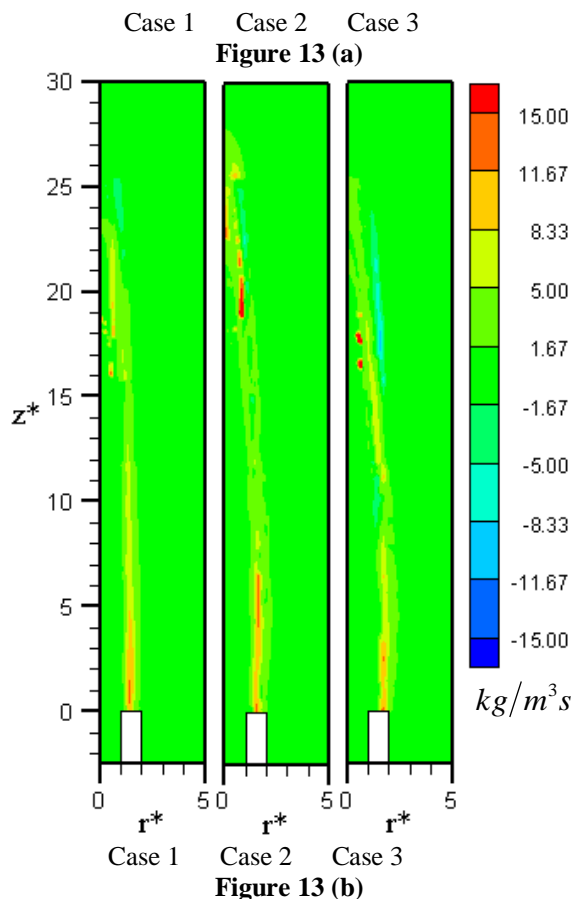
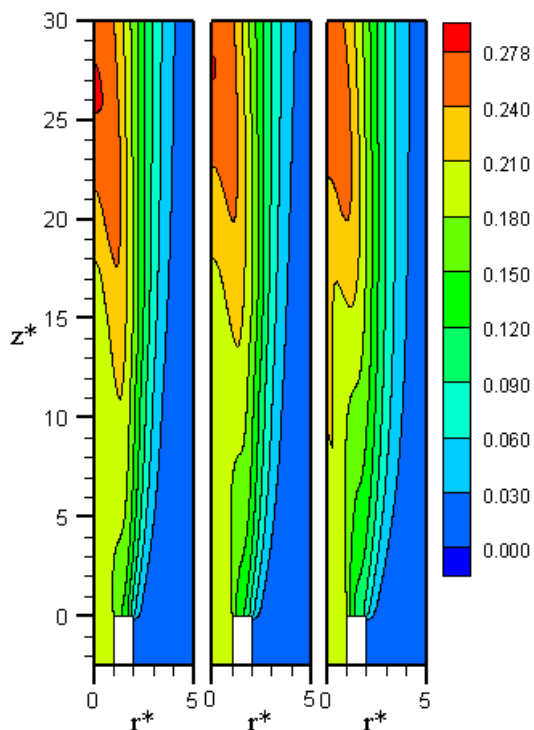


Figure 12 (b)

Figure 12: Contours of (a) mass fraction and (b) net reaction rate of  $\text{O}_2$

of CO<sub>2</sub> in the ambient.

The trends seen for the major species can be summed up as follows: It is apparent (Fig. 7 (a)) that H<sub>2</sub> having low mass fraction is consumed to form both H and OH, primarily through the reaction, H<sub>2</sub>+O=OH+H (chain branching). The OH reactions lead to the formation of H<sub>2</sub>O through the reactions, O+H<sub>2</sub> = OH + H, OH+H<sub>2</sub> = H<sub>2</sub>O+H (chain propagation) and OH + HO<sub>2</sub> = H<sub>2</sub>O+O<sub>2</sub> (chain termination). These occur near the burner exit. CO forms CO<sub>2</sub> with the help of OH, which is an important reaction in CO-H<sub>2</sub> system, given as, CO + OH = CO<sub>2</sub> + H. However, CO<sub>2</sub> (Fig 13.b) formation occurs away from the burner exit but close to the axis, mainly for two reasons; H<sub>2</sub>O reactions are faster, H<sub>2</sub> mass is low and more quantity (by mass) of CO is present, which is basically transported by convection in the axial direction. Thus, hydrogen spreads both axially as well as radially due to its lightness and higher diffusivity. It may also be noted that reverse reactions involving H<sub>2</sub>O+H and CO<sub>2</sub>+H are much slower than the corresponding forward reactions OH+H<sub>2</sub> and CO+OH, mainly because final stable products are seen in the reverse reactions, and they occur near the maximum temperature zone.



**Figure 13:** Contours of (a) mass fraction and (b) net reaction rate of CO<sub>2</sub>

The mass fraction contours and net reaction rates of OH are seen in Figs. 14.(a) and (b). The mass fraction of OH is maximum in the high temperature zone near the burner rim. Here also the similar trend is observed where OH spreads radially outwards (spreads wider) and axially away from the burner exit with the increase in composition of H<sub>2</sub> mass fraction. The following reactions participate to form OH along with the other species H + O<sub>2</sub> = O + OH, HO<sub>2</sub> + H = OH + OH, HO<sub>2</sub> + O = OH + O<sub>2</sub>, H<sub>2</sub>O<sub>2</sub> + O = OH + HO<sub>2</sub>, CO + HO<sub>2</sub> = CO<sub>2</sub> + OH, HCO + O = CO + OH. Both zones of net positive and negative reaction rates are seen which signify zones of OH production and consumption. Atomic hydrogen is a highly active radical and it is capable of diffusing inside the flame zone also. It participates in reactions involving OH outside the flame and in reactions involving CO<sub>2</sub> and CO inside the flame, thus getting distributed in the high reaction zone around the flame. Also the production zone of H becomes thicker (seen in radial direction) and slightly moves away from the burner exit (in axial direction) with increase in percentage of hydrogen mass fraction. It is also seen from Fig 15,



**Figure 14 (b)**

**Figure 14:** Contours of (a) mass fraction and (b) net reaction rate of OH

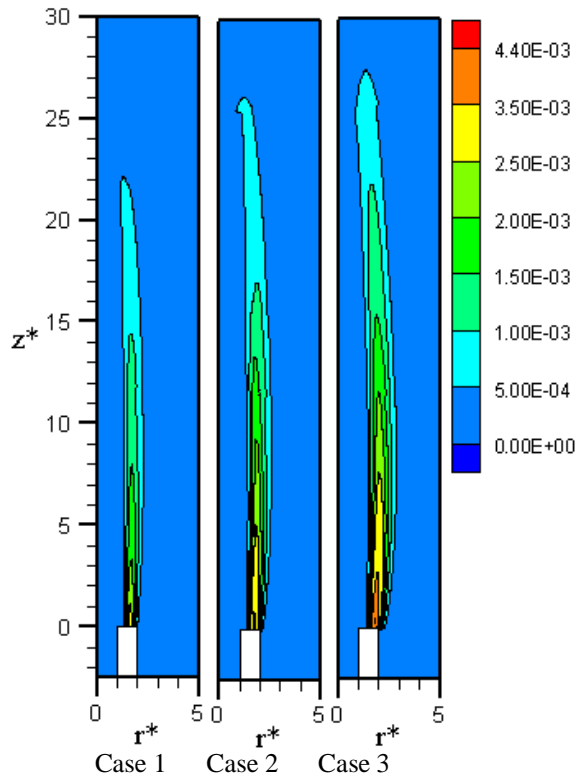


**Figure 14 (a)**

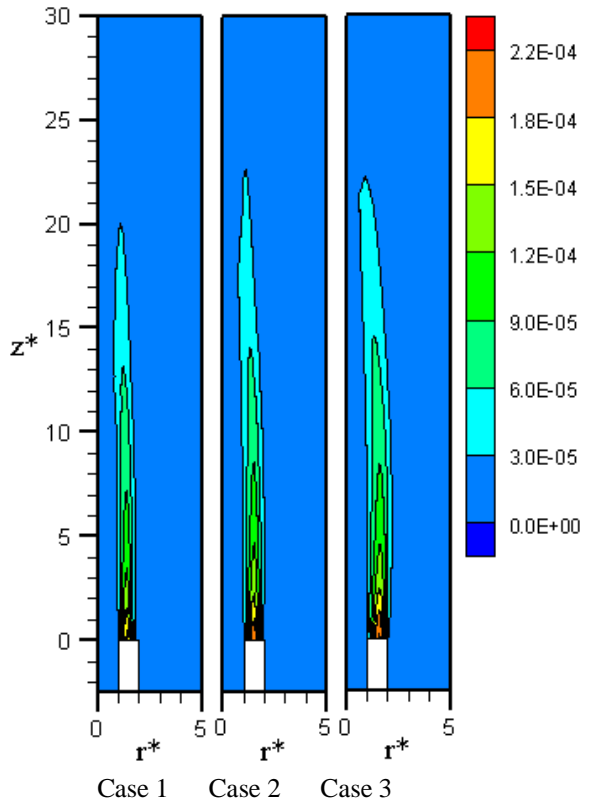
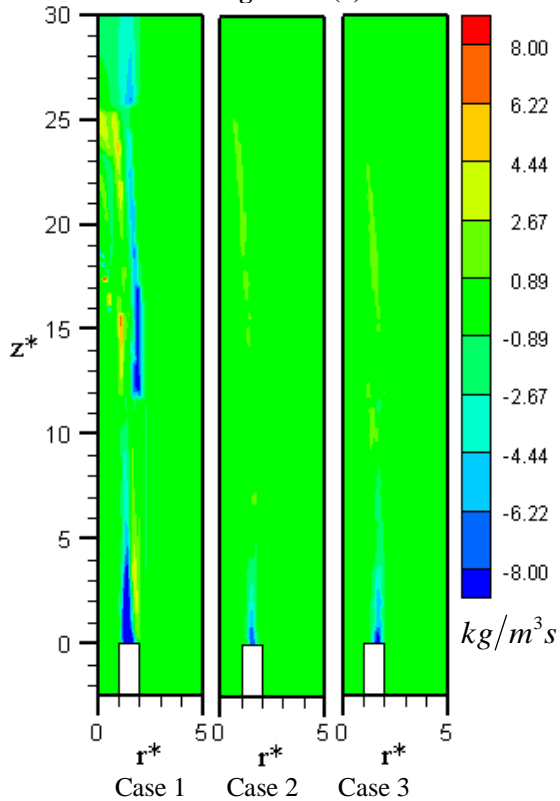


**Figure 15:** Mass fraction of H

that the maximum production of atomic hydrogen occurs at the burner tip. Thus, the reaction involving  $\text{CO} + \text{OH} = \text{CO}_2 + \text{H}$  could be the main step for the production of atomic hydrogen.

### CONCLUSIONS

Syngas combustion in jet diffusion flame mode has been numerically simulated. Basic composition of the syngas has been taken from the product of gasification of Indian coals reported in literature. An axisymmetric model with simplified Davis mechanism [13] has been used to simulate jet diffusion flames fueled by syngas.

The hydrogen content in the fuel mixture has been increased by keeping the fractions of  $\text{CO}_2$  and  $\text{CO}$  the same, by decreasing the nitrogen in the fuel. Three cases have been simulated. A detailed examination of the reaction zone indicates that along the radial direction,  $\text{CO}$  oxidation follows the formation of water vapor by hydrogen oxidation. The higher species diffusivity and kinetic rate coefficient values for the hydrogen-oxygen reaction over those of  $\text{CO}$  play a crucial role in determining the overall syngas

flame characteristics. The structure of the jet diffusion flame and the high temperature locations can be varied by varying the hydrogen content in the fuel mixture. Knowledge of these changes in the flame structure could be of use while designing syngas burners for different gas compositions.

## REFERENCES

- [1] Longwell JP, Rubin ES, Wilson J. Coal: energy for the future. *Prog Energy Combust. Sci*, 21, 1995, 269-360.
- [2] Natarajan J, Kochar Y, Lieuwen T, Seitzman J. Pressure and preheat dependence of laminar flame speeds of H<sub>2</sub>/CO/CO<sub>2</sub>/O<sub>2</sub>/He mixtures. *Proc Combust Inst*, 32, 2009, 1261-1268.
- [3] Hannemann F, Koestlin B, Zimmermann G, Haupt G. Hydrogen and syngas combustion: pre-condition for IGCC and ZEIGCC. *Siemens AG power generation*, W8IN, 2005, G233.
- [4] Brdar R, Jones R. GE IGCC technology and experience with advanced gas turbines. *GE power systems*, Schenectady, NY, 2000 GER-4207.
- [5] Sun, H., Yang SI, Jomaas G, Law CK. High-pressure laminar flame speeds and kinetic modeling of carbon monoxide/ hydrogen combustion. *Proc Combust Inst*, 31, 2007, 439-446.
- [6] Herzler, J., Naumann, C., Shock tube study of the ignition of lean CO/H<sub>2</sub> fuel blends at intermediate temperatures and high pressure. *Combust. Sci. Tech.*, 180, 2008, 2015-2028.
- [7] Dryer FL, Chaos M. Ignition of syngas/air and hydrogen/air mixtures at low temperatures and high pressures: experimental data interpretation and kinetic modeling implications. *Combust Flame*, 152, 2008, 293-299.
- [8] Ichikawa Y, Otawara Y, Kobayashi H, Ogami Y, Kudo T, Okuyama M, et al. Flame structure and radiation characteristics of CO/H<sub>2</sub>/CO<sub>2</sub>/air turbulent premixed flames at high pressure. *Proc Combust Inst*, 33, 2011, 1543-1530.
- [9] Daniele S., Jansohn P, Mantzaras J, Boulouchos K. Turbulent flame speed for syngas at gas turbine relevant conditions. *Proc Combust Inst*, 33, 2011, 2937-2944.
- [10] Frassoldati A, Faravelli T, Ranzi E. The ignition, combustion and flame structure of carbon monoxide/hydrogen mixtures. Note 1: detailed kinetic modeling of syngas combustion also in presence of nitrogen compounds. *Int J. Hydrogen Energy*, 32, 2007, 3471-3485.
- [11] Sung CJ, Law CK. Fundamental combustion properties of H<sub>2</sub>/CO mixtures: ignition and flame propagation at elevated pressures. *Combust. Sci. Technol.*, 180, 2008, 1097-1116.
- [12] Chaos M, Dryer FL. Syngas combustion kinetics and applications. *Combust Sci Technol*, Vol. 180, 2008, pp. 1053-96.
- [13] Davis SG, Joshi AV, Wang H, Egolfopoulos F. An optimized kinetic model of H<sub>2</sub>/CO combustion. *Proc Combust Inst*, 30, 2005, 1283-1292.
- [14] Law CK, Jomaas G, Bechtold JK. Cellular instabilities of expanding hydrogen/propane spherical flames at elevated pressures: theory and experiment. *Proc. Combust. Inst.*, 30, 2005, 159-167.
- [15] Tahtouh T, Halter F, Samson E, Mounaim-Rousselle C. Effects of hydrogen addition and nitrogen dilution on the laminar flame characteristics of premixed methane-air flames. *Int. J. Hydrogen Energy*, 34, 2009, 8329-8338.
- [16] R. K. Iyengar and R. Haque. Gasification of high-ash Indian coals for power generation. *Fuel Processing Technol.*, 27, 1991, 247-262.